Temporal and Spatial Variability in Contemporary Greenland Warming (1958–2020)

QINGLIN ZHANG,[a] BAOJUAN HUAI,[a] MICHIEL R. VAN DEN BROEKE,[b] JOHN CAPPELEN,[c] MINGHU DING,[d] YETANG WANG,[a] AND WEIJUN SUN[a]

[a] *College of Geography and Environment, Shandong Normal University, Jinan, China*
[b] *Institute for Marine and Atmospheric Research, Utrecht University, Utrecht, Netherlands*
[c] *Danish Meteorological Institute, Copenhagen, Denmark*
[d] *State Key Laboratory of Severe Weather, Chinese Academy of Meteorological Sciences, Beijing, China*

(Manuscript received 21 April 2021, in final form 6 January 2022)

ABSTRACT: In this study, 2-m or near-surface air temperature (T2m) products from atmospheric reanalysis ERA5 and the regional climate model RACMO2.3p2 over Greenland are compared with observations from staffed stations and Automated Weather Stations (AWS). The results show the following: 1) Greenland experienced decadal periods of both cooling and warming during 1958–2020, with an inflection point around the mid-1990s, and no significant warming after ~2005 except in the north and northeast. 2) In the full time series, the magnitude of the warming increases gradually from south to north, with peak warming found along the northeastern coast. 3) The most intense warming occurred in autumn and winter, notably in the northeast. 4) The correlations of T2m with the large-scale circulation indices NAO and GBI are highly significant, but they gradually weaken from southwestern to northeastern Greenland. Under the background of Greenland rapidly warming, the shift from positive to negative NAO (negative to positive GBI) is critical to the sudden warming in Greenland since the mid-1990s.

KEYWORDS: Atmospheric circulation; Arctic; Climate variability; Temperature

1. Introduction

The recent widespread mass loss of the Greenland ice sheet (GrIS) has attracted worldwide attention, especially during the warm and high-melt summers of 2012 and 2019 (Nghiem and Coauthors 2012; Tedesco and Fettweis 2020; Hanna et al. 2021). To understand GrIS melt magnitude, it is crucial to understand Greenland 2-m (or near surface) air temperature (T2m) changes, because they determine to a large extent the length and intensity of the melt season. The U.S. National Oceanic and Atmospheric Administration (NOAA) has published updated data on Greenland T2m and mass balance in the Arctic Report Card every year since 2006 (e.g., Moon et al. 2020). In the context of global warming, Arctic amplification is significant: the Arctic has become the fastest-warming region in the world (Serreze and Francis 2006), and Greenland T2m has significantly increased relative to the twentieth century. In this study, we demonstrate that this warming has been highly heterogeneous in time and space.

Currently there are three major climate networks in Greenland: the Danish Meteorological Institute (DMI) network of staffed and automatic meteorological stations in the ice-free parts of the island, situated mainly at coastal locations (Cappelen 2021); the Greenland Climate Network (GC-Net) operating Automatic Weather Stations (AWS) mainly in the interior (accumulation zone) of the ice sheet (Steffen et al. 1996); and the Program for Monitoring the Greenland Ice Sheet (PROMICE), which operates stations mainly in the GrIS ablation zone (Fausto et al. 2021; Colgan et al. 2019). The latter two networks will be gradually merged into an extended PROMICE AWS network in the course of the coming years. In addition, the Greenland Ecosystem Monitoring network (GEM; Christensen et al. 2018), focusing on detailed studies in several carefully selected locations, and Asiaq Greenland have both made important contributions to Greenland climate and ecosystem monitoring.

Based on these near-surface meteorological observations, multiple studies have been published on T2m conditions and trends in Greenland. Hanna and Cappelen (2003) found that southwestern Greenland cooled by 1.3°C from 1958 to 2001, based on data of eight DMI stations. Box et al. (2009), Hanna et al. (2012), Jiang et al. (2020), and Hanna et al. (2021) updated the time range of temperature changes to 2007, 2012, 2017, and 2019, respectively. However, studies based on AWS data alone are often limited by the relative brevity of the time series and the reduced quality of unsupervised observations, resulting in data gaps. The station spatial coverage is also limited, particularly in eastern Greenland (e.g., Jiang et al. 2020). Cappelen et al. (2001) shows that numerous regional microclimates exist in Greenland, further hampering the interpretation of station data in the context of the wider regional temperature change.

New technologies and methods such as satellite remote sensing, atmospheric reanalyses, and regional climate models can be used to fill in gaps in both space and time (e.g., Dethloff et al.

Denotes content that is immediately available upon publication as open access.

Supplemental information related to this paper is available at the Journals Online website: https://doi.org/10.1175/JCLI-D-21-0313.s1.

Corresponding authors: Baojuan Huai, huaibaojuan@126.com; Weijun Sun, sun1982wj@163.com

DOI: 10.1175/JCLI-D-21-0313.1

1996; Comiso 2003; Hanna et al. 2008; Fettweis et al. 2017; Noël et al. 2018). Although models provide complete spatial and temporal coverage of T2m, different downscaling and parameterization schemes will affect the performance of the results. Even when all observations are assimilated, which is not always the case, the limited spatial coverage of multidecadal instrumental sites, especially on the inland ice sheet and in the north, means that atmospheric reanalyses remain relatively unconstrained (Orsi et al. 2017). Reeves Eyre and Zeng (2017) evaluated and compared T2m from 16 datasets over Greenland, including reanalysis data from MERRA-2, ERA-Interim, CFSR, and output of the Modèle Atmosphérique Régional (MAR), and found that their performance differs by season and region. MERRA2 shows the largest T2m trend in the southwest during 1980–2008, while three MAR versions forced by ERA-40, ERA-Interim, 20CRv2c, and ERA-20C respectively, have their largest trends in the northeast. As a result, for multiple Greenland regions and epochs, T2m change remains largely unclear.

In this paper, we present Greenland T2m conditions during 1958–2020 after evaluating the ECMWF reanalysis products ERA5 and the regional climate model RACMO2.3p2 (henceforth RACMO2), developed specifically for use over glaciated regions (Noël et al. 2015). Based on this evaluation, we use the RACMO2 data to study the influence of large-scale atmospheric circulation variability on T2m, especially the North Atlantic Oscillation (NAO) and high pressure blocking over Greenland [Greenland blocking index (GBI); Hanna et al. 2016]. We aim to address the following questions: 1) How has Greenland T2m changed over the period 1958–2020? 2) What is the regional variability of T2m changes? 3) How do the impacts of NAO and GBI vary by region? This paper is structured as follows: The data and methods are described in sections 2 and 3, respectively. ERA5 and RACMO2 modeled T2m are evaluated in section 4a; section 4b presents the Greenland T2m changes during the period 1958–2020; and section 4c discusses the correlation of NAO and GBI circulation indexes T2m over Greenland, followed by a discussion in section 5. Conclusions are presented in section 6.

2. Data

a. Observational air temperature data

We use daily and monthly T2m data of 20 meteorological stations from the PROMICE network and daily T2m observations from nine DMI automated and staffed weather stations. The distribution of meteorological stations over Greenland is shown in Fig. 1 using the polar stereographic projection. The location, elevation and the observational period from these stations are listed in Table 1. For DMI observations, only when availability of valid daily data is $> 80\%$, monthly T2m is calculated, and the seasonal and annual T2m are calculated only when all monthly data are available. GC-Net data have been assimilated in ERA5, but not PROMICE data (Delhasse et al. 2020), and therefore the performance of ERA5 and RACMO2 can be objectively evaluated using the PROMICE data. On the other hand, we were informed by ECMWF technical support (H. Hersbach 2021, personal communication) that some DMI station data have been assimilated in ERA5 (e.g., Upernavik, Nuuk, Tasiilaq, Danmarkshavn, and Qaqortoq). Therefore, we decided not to use GC-net and DMI observations for evaluation.

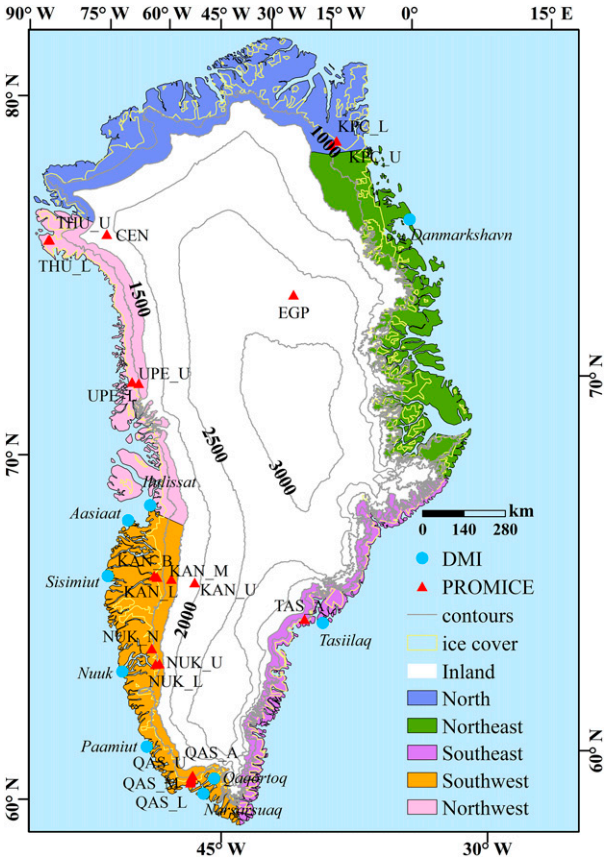

FIG. 1. Map of the study area and locations of weather stations used in this work: blue circles are DMI stations marked in italics, and red triangles are PROMICE AWS. The yellow outline represents the ice cover, and Greenland is divided into six regions. The inland is defined as contiguous ice-covered regions above 1500 m approximately representing the altitude of the equilibrium line.

b. ERA5

The fifth-generation ECMWF reanalysis ERA5 has a spatial resolution of 0.25° and a time resolution of 1 h and has replaced ERA-Interim for all practical purposes (Hersbach and Dee 2016). ERA5 runs from 1950 to the present and was first released in October 2020 (Bell et al. 2020). The number of vertical levels in ERA5 is 137; 4D-VAR data assimilation was improved, and more observations were assimilated (ECMWF 2018). In this study, we use daily and monthly means of T2m from ERA5 (1958–2020).

c. RACMO2.3p2

The regional climate model RACMO2.3p2 was developed by the Royal Netherlands Meteorological Institute (KNMI) and adapted for polar glaciated regions at the Institute for Marine

TABLE 1. Overview of the AWS used in this study (stations in italics indicate that they are from DMI; other stations are from PROMICE).

Station name	Lat (°N)	Lon (°W)	Elev (m)	Data period used in this study
Danmarkshavn	76.77	18.67	11	Jan 1958–Dec 2020
Tasiilaq	65.60	37.62	53	Jan 1958–Dec 2020
Qaqortoq	60.72	46.05	32	Jan 1961–Dec 2020
Narsarsuaq	61.17	45.42	27	Jan 1961–Dec 2020
Paamiut	62.02	49.67	36	Jan 1958–Dec 2020
Nuuk	64.17	51.75	80	Jan 1958–Dec 2020
Aasiaat	68.70	52.75	43	Jan 1958–Dec 2020
Ilulissat	69.23	51.07	29	Jan 1961–Dec 2020
Sisimiut	66.95	53.72	10	Jan 1961–Dec 2020
KPC_L	79.91	24.08	370	Jul 2008–Dec 2020
KPC_U	79.83	25.17	870	Jul 2008–Dec 2020
EGP	75.62	35.97	2660	May 2016–Dec 2020
TAS_A	65.78	38.90	890	Aug 2013–Dec 2020
QAS_L	61.03	46.85	280	Aug 2007–Dec 2020
QAS_M	61.10	46.83	630	Aug 2016–Dec 2020
QAS_U	61.18	46.82	900	Aug 2008–Dec 2020
QAS_A	61.24	46.73	1000	Aug 2012–Aug 2020
NUK_L	64.48	49.54	530	Aug 2007–Dec 2020
NUK_U	64.51	49.27	1120	Aug 2007–Dec 2020
NUK_N	64.95	49.89	920	Jul 2010–Jul 2014
KAN_B	67.13	50.18	350	Apr 2011–Dec 2020
KAN_L	67.10	49.95	670	Sep 2008–Dec 2020
KAN_M	67.07	48.84	1270	Sep 2008–Dec 2020
KAN_U	67.00	47.03	1840	Apr 2009–Dec 2020
UPE_L	72.89	54.30	220	Aug 2009–Dec 2020
UPE_U	72.89	53.58	940	Aug 2009–Dec 2020
THU_L	76.40	68.27	570	Aug 2010–Dec 2020
THU_U	76.42	68.15	760	Aug 2010–Dec 2020
CEN	77.17	61.11	1880	Jul 2017–Dec 2020

and Atmospheric Research, Utrecht University (IMAU/UU), specifically to simulate the climate and surface mass balance of the ice sheets of Antarctica and Greenland (Noël et al. 2015, 2018). In Greenland, the glacier outlines and surface topography are prescribed from the Greenland Ice Sheet Mapping Project (GIMP) digital elevation model (Howat et al. 2014). Detailed information about RACMO2 including the snow module and the improvement of surface parameterization schemes can be found in Noël et al. (2018). Here we use the outputs with a spatial resolution of 5.5 km and 40 vertical layers. In the dataset used here, the lateral atmospheric boundaries of RACMO2.3p2 were forced at 6-hourly time intervals by ERA-40 for the period 1958–78 and by ERA-Interim for the period 1979–2018 and at 3-hourly time intervals by ERA5 for the period 2019–20. The sea surface temperature (SST) and sea ice cover in model are prescribed from the same reanalysis data that force RACMO2 at the lateral and top boundaries.

d. GBI and NAO index

The Greenland blocking index represents the mean 500-hPa geopotential height for the region 60°–80°N, 20°–80°W (Fang 2004; Hanna et al. 2015, 2016). The NAO index represents the normalized sea level pressure (SLP) difference between Iceland and the Azores (Rogers 1984; Hurrell 1995; Jones et al. 1997). In this study, we used the NAO index calculated from pressure measured in Gibraltar and southwestern Iceland (Jones et al. 1997).

3. Methods

Before using the model results for T2m analysis, RACMO2 and ERA5 were evaluated using observations. We calculate the correlation coefficient R, root-mean-square error (RMSE), mean bias (hereinafter "BIAS"), and mean absolute error (MAE) between daily and monthly T2m observations and each model dataset. Modeled values of T2m are computed for each meteorological station location using bilinear interpolation of the four surrounding land grid points. For evaluation purposes, we cleared RACMO2 and ERA5 data for periods of missing observations. Note that, when evaluating monthly data, if the number of daily averages from PROMICE is less than the complete month then the average of that month is not calculated.

To assess regional differences in T2m changes, Greenland is divided into six regions (Fig. 1) based on the 1500-m contour and drainage basins (van den Broeke et al. 2009). For long T2m time series, the detection of breakpoints is often useful for the analysis of interdecadal trend differences. Here we use Pettitt's test (Pettitt 1979), a nonparametric test that has been widely applied in detecting the presence of abrupt changes in climatic data (e.g., Ilori and Ajayi 2020; Espinoza et al. 2019).

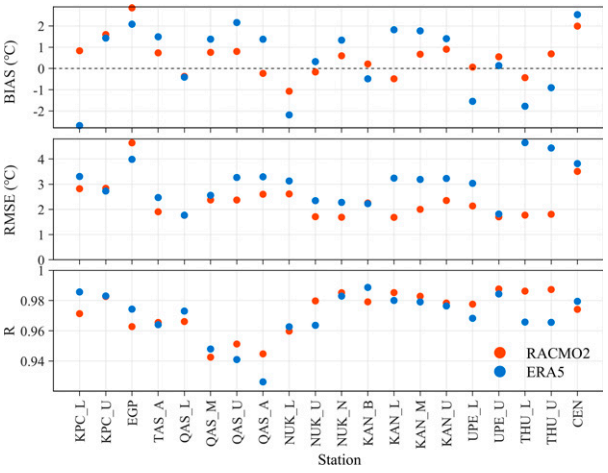

FIG. 2. Correlation coefficients R, mean difference (BIAS), and root-mean-square error (RMSE) of daily meanT2m in ERA5 and RACMO2. KAN_B is located on land, and the rest of the stations are located on the GrIS.

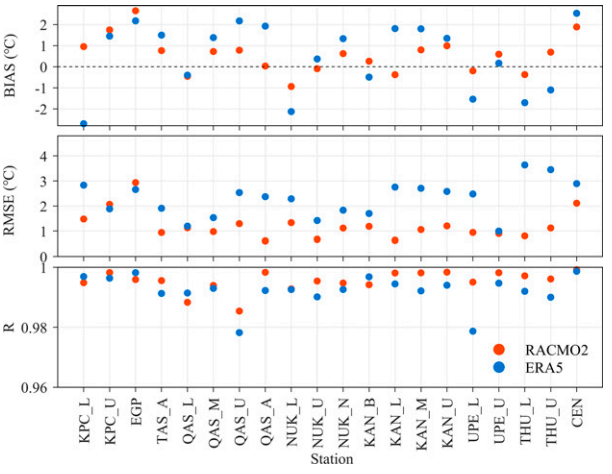

FIG. 3. As in Fig. 2, but for monthly T2m.

In this study, Pettitt's test is used to find a significant inflection year in the regional T2m time series from RACMO2 and ERA5. Both RACMO2 and ERA5 are subjected to this test, and the results are compared to reflect the T2m change as objectively as possible. Furthermore, a time-varying trend analysis is utilized for revealing different trends in subperiods. The spatial distribution of the correlation and linear regression slope between linearly detrended T2m and NAO or GBI in different periods is used to show the close relationship between T2m changes and large-scale circulation indices.

4. Results

a. Evaluation of ERA5 and RACMO2

The evaluation results of ERA5 and RACMO2 are shown in Fig. 2 (daily averages) and Fig. 3 (monthly averages). The overall performance of ERA5 and RACMO2 is aggregated in Table 2 using the average values of R, RMSE, and MAE of all stations. For daily average T2m, both datasets show high correlations, with $R > 0.93$ ($p < 0.05$) and mean $R > 0.96$. Except for EGP and CEN located at high altitude on the ice sheet, RMSE of RACMO2 is < -3°C and BIAS is < 2°C at all stations. Relative to daily data, all performance indicators of monthly average T2m further improve, especially R (>0.97; $p < 0.05$) with an average of >0.99. RAMCO2 generally outperforms ERA5 with mean RMSE and MAE values approximately one-half of that of ERA5, demonstrating that regional downscaling and dedicated model physics do improve the quality of the simulated T2m. Note that these statistics based on daily and monthly averages depend strongly on the length of the observational period. Varying the averaging time interval, for instance, at the K-transect (see Fig. S1 in the online supplemental material) shows that the model performance does not improve significantly farther beyond the 30-day time interval. Based on these results, in the following discussion primarily RACMO2 data will be used to study recent T2m change in Greenland. The ERA5 data are on several occasions used for comparison.

b. Greenland T2m climatology

Figure 4 shows the annual mean T2m anomalies relative to the full period average (1958–2020), spatially averaged for six different regions (Fig. 1) and for the whole of Greenland. A major result is that all regions first experienced a cooler followed by a warmer period, with a significant jump that occurred around the mid-1990s (the orange vertical line in Fig. 4). This abrupt change is also found in time series of GrIS surface mass balance, which has been decreasing since the 1990s (Noël et al. 2020), and in summer [June–August (JJA)] GrIS shortwave and longwave downward radiation since mid-1990s (Hofer et al. 2017). Noël et al. (2019) found a similar jump in GrIS integrated meltwater runoff in 1990. The reason for the difference in timing between T2m and meltwater runoff inflection year could be the eruption of the volcano Pinatubo in 1991 (McCormick et al. 1995), having a well-established cooling influence in Greenland (Abdalati and Steffen 1997).

We find that the jump in T2m is timed differently from region to region, with northern Greenland warming slightly earlier than the south. The magnitude of the jump in T2m (Fig. 5a) shows a clear north–south difference, becoming progressively greater with increasing latitude, with the maximum difference occurring in the north. This north–south difference is evident in all seasons except JJA (Fig. 6), consistent with Abermann et al. (2017). For JJA, warming of about 1.25°C is found in both inland and coastal regions. Meanwhile, the

TABLE 2. The average evaluation index values of R, RMSE, and MAE.

	Daily data			Monthly data		
	MAE	RMSE	R	MAE	RMSE	R
ERA5	2.4	3.1	0.967	2.0	2.3	0.992
RACMO2	1.7	2.3	0.971	1.0	1.2	0.995

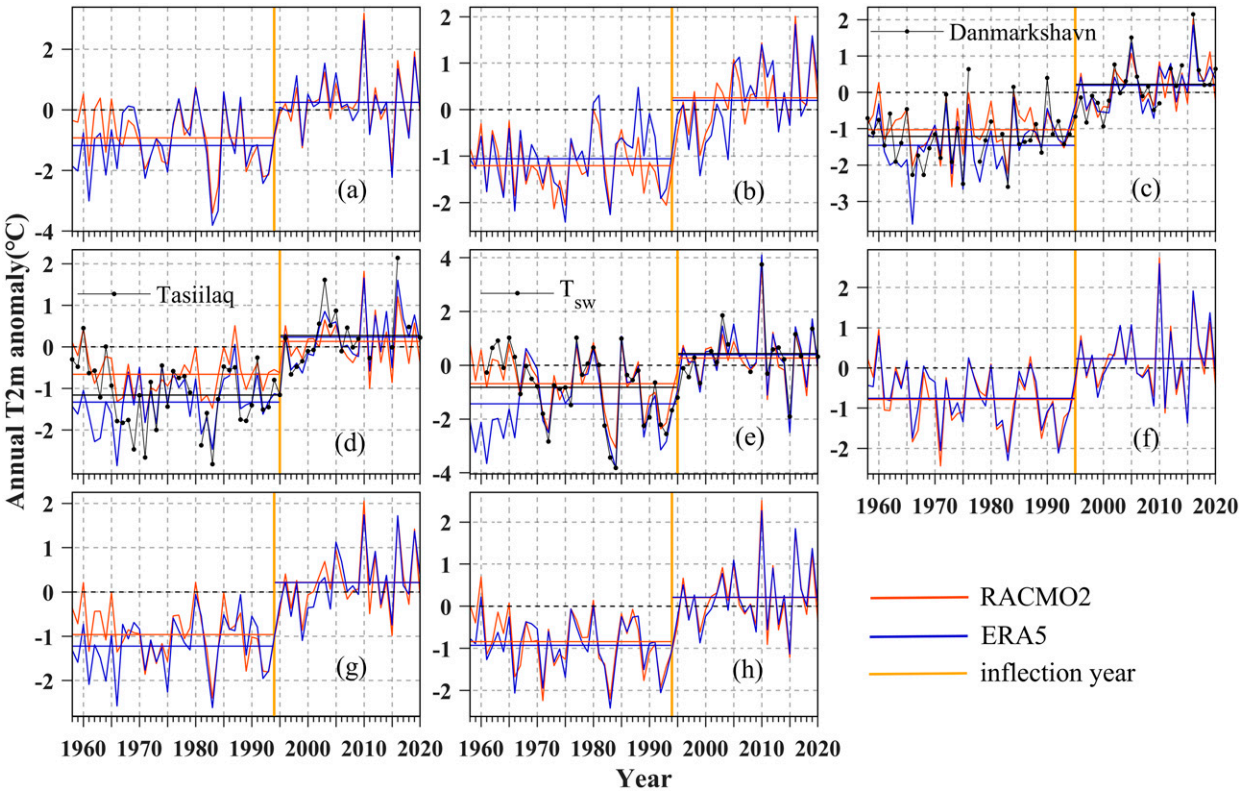

FIG. 4. Time series of mean annual T2m anomaly relative to the 1991–2020 base period in different regions of Greenland: (a) northwest, (b) north, (c) northeast, (d) southeast, (e) southwest, (f) inland, (g) coastal area, and (h) all of Greenland. The red and blue lines represent RACMO2 and ERA5, respectively. The orange line represents the inflection year passing a 0.05 significance level test. The red and blue horizontal lines represent mean anomalies of RACMO2 and ERA5 in different periods, respectively. The black solid lines in (c) and (d) represent observations of Danmarkshavn and Tasiilaq. In (e), T_{sw} represents the mean data of six stations in the southwest: Aasiaat, Nuuk, Paamiut, Narsarsuaq, Qaqortoq, and Sisimiut.

strong warming in September–November (SON) and December–February (DJF) in the northeast is the reason for the fastest annual T2m warming in this region.

The rapid warming in the first 10 years after the mid-1990s is consistent with the study of Chylek et al. (2006). Since then, the temperature remained at this higher level, but the positive trends have declined since then except in the north and northeast, as also reported in a previous study (Hanna et al. 2021). Annual Greenland T2m calculated by the average of all Greenland grid points from RACMO2 has been 1°C higher since the transition, with many historical high values including model and record values (e.g., 2010 and 2016) occurring since, as proved by Mernild et al. (2014).

In Fig. 5b we show T2m anomalies for two exceptionally warm years (2010 and 2016), with a T2m anomaly in excess of 2 standard deviations above the long-term mean, and two cold years (1983 and 1992), likely influenced by volcanic eruptions. In 1983 and 1992, the negative T2m anomaly in western Greenland was greater than that in eastern Greenland. The year 2010 was the warmest year in all regions except for the north and northeast, and the most anomalously warm region is the southwest, as indicated by numerous observational temperature recorded values (Box et al. 2011). High GBI values in spring [March–May (MAM)] 2010 and the previous winter (DJF 2009/10) indicate strong blocking, which resulted in a warm first few months of 2010 (Hanna et al. 2016). Consistent with the regional differences shown in Fig. 4, northern and northeastern Greenland were the most anomalously warm areas in 2016. As compared with the annual T2m, surface melt over the ice sheet occurs mainly in summer and therefore is more relevant to dampen swings in summer T2m, especially in the warm summers of 2012 and 2019. The mean JJA 2012 T2m anomaly in RACMO2 was above 1°–1.5°C for almost all of Greenland and even reached 2.5°C in the south and southwest with respect to mean JJA 1991–2020. This extensive warming anomaly corresponds to the maximum melting extent of 98.6% in the summer of 2012 (Nghiem and Coauthors 2012). In contrast, the positive temperature anomaly in the summer of 2019 is mainly concentrated in the southwest and north because of the exceptional persistence of a high pressure system centered near Summit (Tedesco and Fettweis 2020).

With only few complete temperature records over 63 years available, the monthly fields from RACMO2 were used to map T2m trends over Greenland. We divided the time series into two periods before and after the temperature jump,

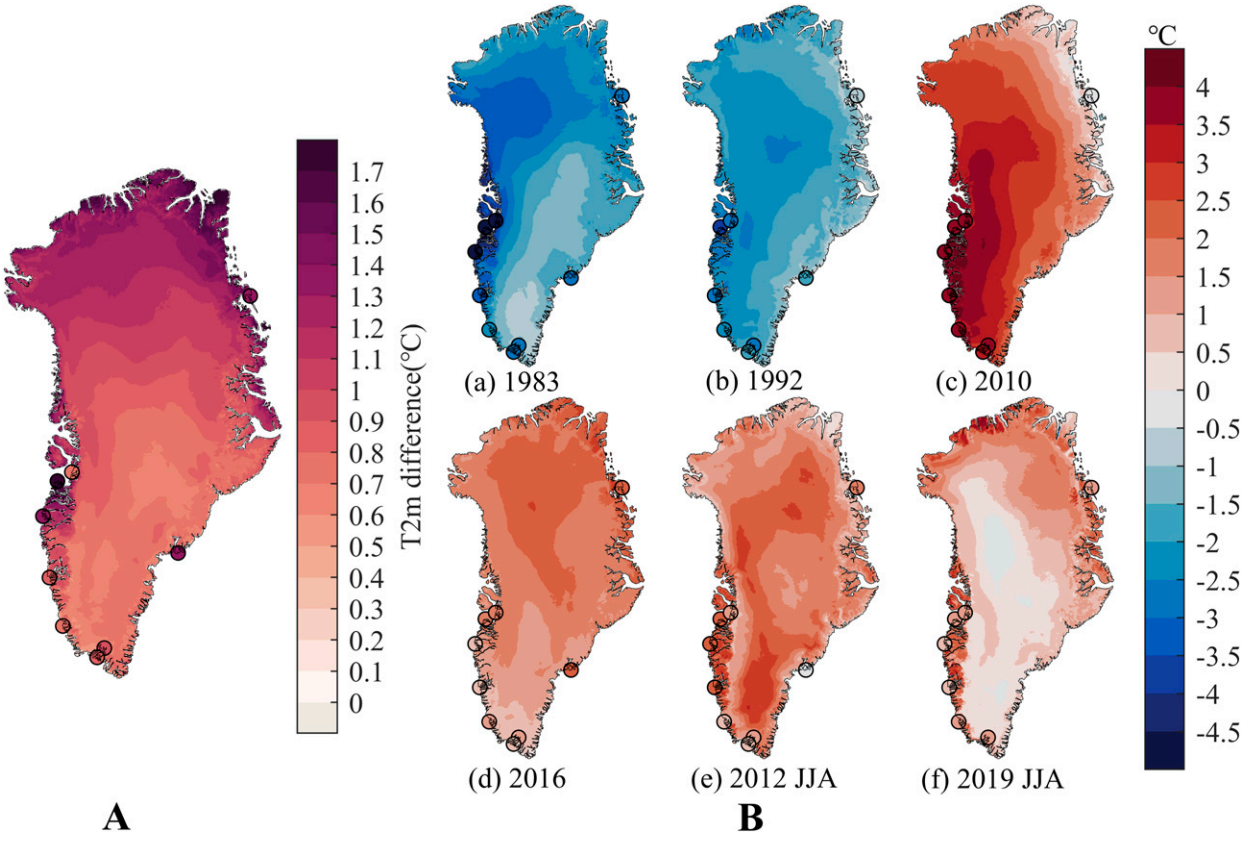

FIG. 5. (left; label A) RACMO2 T2m difference (°C) between the two periods before and after the temperature jump. Note that 1994 is chosen as the jump year. (right; label B) Annual T2m anomalies (°C) for (a) 1983, (b) 1992, (c) 2010, and (d) 2016, with respect to mean annual 1991–2020, and JJA T2m anomalies (°C) for (e) 2012 and (f) 2019 with respect to mean JJA 1991–2020. The dots represent the DMI stations, using the same color scale.

1958–93 and 1994–2020. Figure 7 shows the spatial distribution of T2m trends over the full period (left) and for 1958–93 (right) for (top) RACMO2 and (bottom) ERA5. For the entire 63 years, RACMO2 suggests that the north is warming faster than the south. During 1958–93, the strongest cooling in the RACMO2 results is in the southwest, consistent with the stations result shown in Fig. 7, and supported by previous studies (e.g., Hanna and Cappelen 2003; Hanna et al. 2008; Box 2002; Box et al. 2009). Conversely, ERA5 suggests that the ice-free tundra around the entire island warmed before 1994. The reason for this difference is that ERA5 underestimates T2m in the southeast and southwest before the mid-1960s, as shown in Figs. 4d and 4e. In addition, the results of time-varying trends (Fig. 8) showed that 1992–2003 was the most significant period of warming (1.1°–2.4°C decade^{-1}) for all regions of Greenland. The patterns for the northwest and southwest show consistency, both in the cooling and the warming period. Although in this study the 63-yr-long time series is divided into two climatic periods, there are also insignificant trends of T2m increase or decrease in cooling or warming subperiods, respectively. In all regions, significant warming occurred in the 1970s, with subsequent cooling periods over Greenland except the northeast and southeast regions. We also found that after 2003 western Greenland showed a nonsignificant cooling.

The results (shown in Figs. S2 and S3 in the online supplemental material) of using another inflection point (1995) show that there is little difference between using 1994 and 1995 as the uniform inflection year. Therefore, we continue to use 1994 as the uniform inflection year in the following.

c. *Regional variability in the influence of large-scale circulation*

In general, except for the northeast coast of Greenland, observations and RACMO2 show that in all seasons Greenland T2m during 1958–2020 is positively correlated with GBI and negatively correlated with NAO (Figs. S4 and S5 in the online supplemental material). Spatially, this correlation weakens from south to north and from west to east. Regardless of the season and period, the southwest is the region with the most significant correlation with the NAO or GBI. The correlation between T2m and NAO or GBI differs for different periods. During the period 1958–93, the correlation between NAO or GBI and temperature was most significant in DJF with 60% or 53%, respectively, of Greenland $R > 0.6$. Since the warming jump, this correlation has broadly increased, especially in MAM and JJA. For instance, for JJA, NAO R increased its magnitude (i.e., became more negative) by 0.29 on

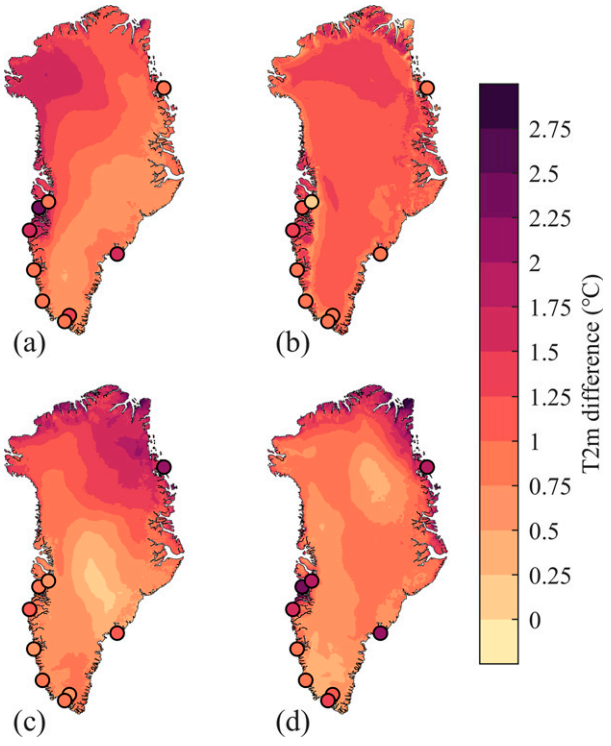

FIG. 6. RACMO2 T2m difference (°C) before and after the temperature jump, in (a) MAM, (b) JJA, (c) SON, and (d) DJF. 1994 is chosen as the jump year. The dots represent DMI stations using the same color scale.

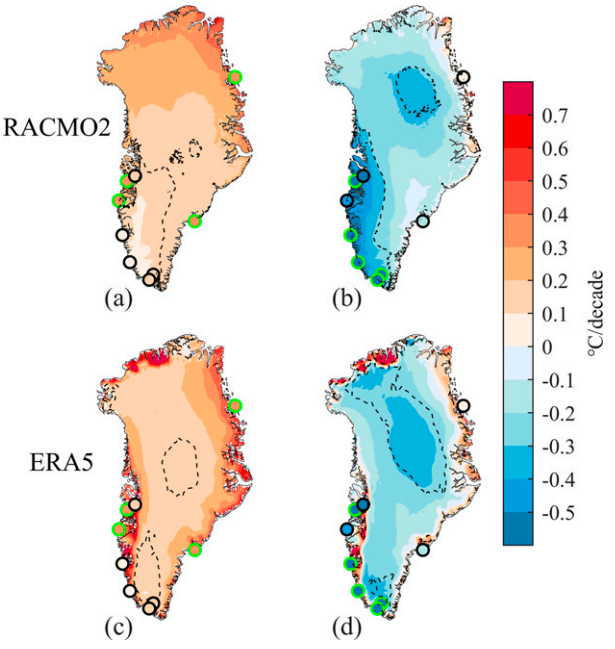

FIG. 7. Map of annual T2m trend (°C decade^{-1}) from RACMO2 during (a) 1958–2020 and (b) 1958–93 and from ERA5 during (c) 1958–2020 and (d) 1958–93. The dashed line indicates represents the 95% significance level contour. The dots represent the DMI stations, and the color represents the results of the station data. For stations, the green circle indicates that the trend passes the 95% significance test.

average. This suggests that in a background warming climate, T2m in Greenland has become more sensitive to variability in circulation, as reported by Hanna et al. (2021).

To further quantify this relationship, we used linear regression to calculate the corresponding change in T2m for a 1 standard deviation change in NAO and GBI (Figs. 9 and 10). The season with the strongest T2m response is winter, especially in southwestern Greenland. For instance, both RACMO2 and observations show that the southwest warms 3.2°C per σ GBI (Figs. 9d,h). The slope magnitudes for NAO are generally smaller than for GBI (Fig. 10). Furthermore, except for MAM and JJA, the sensitivity of T2m for NAO variability is weakening, in contrast to GBI. The main reason for the loss of correlation with NAO but not with GBI is that since the 1990s the GBI shows a significantly increasing trend for most seasons whereas the NAO decrease is mostly restricted to summer (Hanna et al. 2015). The regions with strong T2m response to the GBI extend northward, which may be related to the northward movement of the blocking (Rajewicz and Marshall 2014; McLeod and Mote 2016). We conclude that, when compared with NAO, Greenland blocking, as a local circulation feature in Greenland, has a more direct and strong impact on T2m. In the context of recent warming, with the increase of anticyclonic weather under the influence of blocking (Hanna et al. 2018; Tedesco et al. 2016; Tedesco and Fettweis 2020), the GBI is expected to contribute more to Greenland warming than the NAO. In addition, the response of T2m to NAO and GBI in the northeast is weaker than that in other regions, and even shows an opposite sign in some seasons, like MAM for GBI (Fig. 9a) and SON for NAO (Fig. 10g).

5. Discussion

It is well established that Greenland T2m is strongly influenced by interannual to decadal variability in Greenland blocking, expressed by the GBI, and the NAO (Fettweis et al. 2013; van den Broeke et al. 2017; Hofer et al. 2017). GBI and NAO are highly negatively correlated (Davini et al. 2012). When NAO changes from a negative to a positive phase, this leads to a reduction of warm air transport to western Greenland (Buch et al. 2004). At the same time, northwestern Europe will get warmer, which is often referred to as the temperature seesaw (van Loon and Rogers 1978). In contrast, the positive phase of GBI constitutes high pressure blocking and anticyclonic weather (Hanna et al. 2018), with southwesterly winds transporting warm air masses northward (Mioduszewski et al. 2016), leading to a warm phase, especially in western Greenland.

In this study we report a significant jump in Greenland near-surface air temperature (T2m) around 1994, with relatively stable temperatures in the periods before (1958–93) and after (1994–2020). Exceptions are the north and northeast of Greenland, where the latter period shows continued warming. Large-scale atmospheric circulation variability can effectively

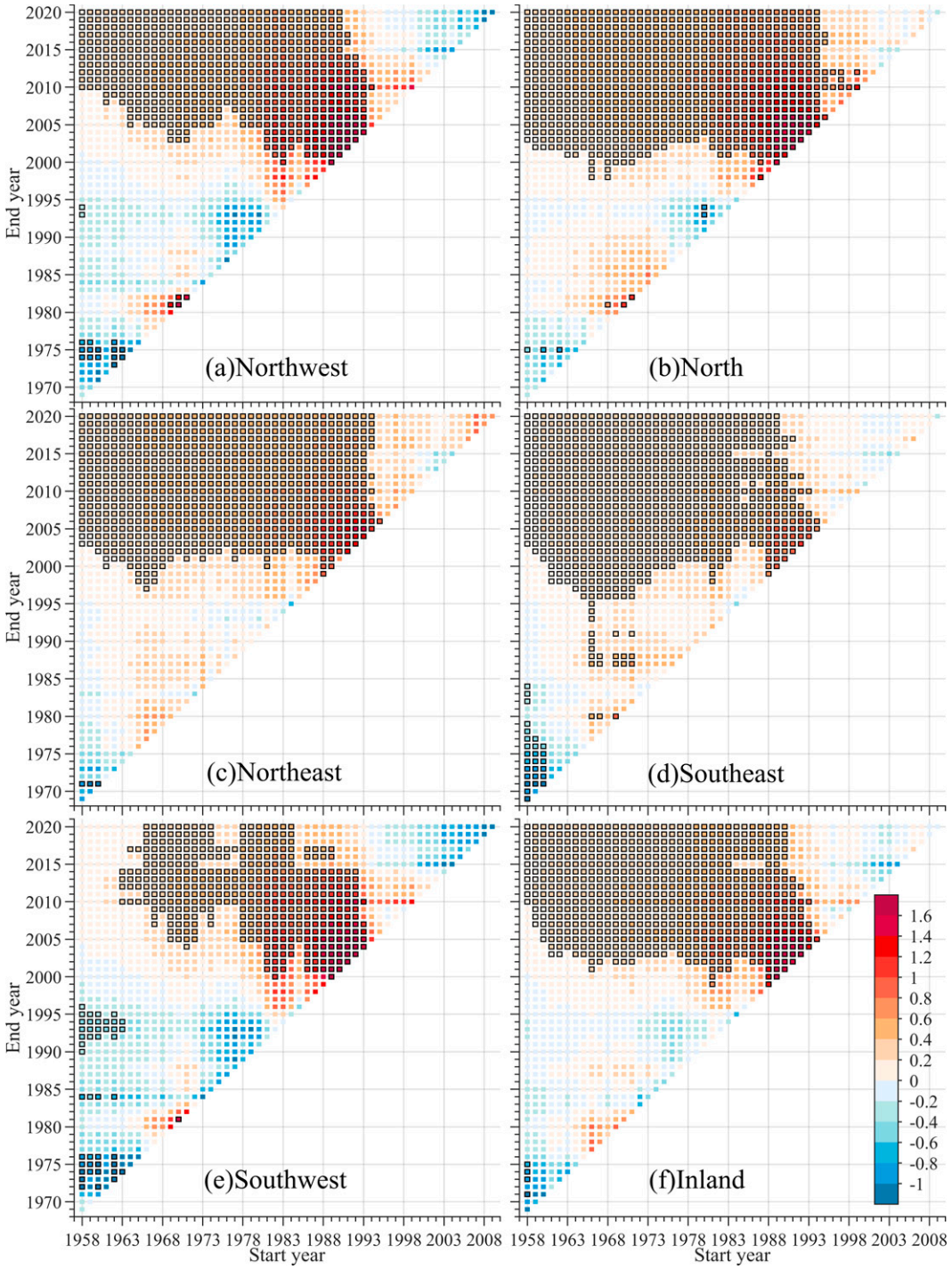

FIG. 8. Trends of the (a) northwest, (b) north, (c) northeast, (d) southeast, (e) southwest, and (f) inland areas in each period. Black-outlined squares indicate statistical significance at greater than 95% confidence level.

explain this interdecadal variability of Greenland T2m. Figure 11 shows time series (1958–2020) of annual mean GBI and NAO. Until the mid-1980s, the magnitude of both indices was relatively small and variations mainly of interannual nature. For the decade between the early 1980s and the early 1990s, the GBI and NAO indices respectively became significantly negative and positive, coinciding with the cool phase in most of Greenland. In addition, before the warming jump in 1994, there were several large volcanic eruptions, like Agung (1963), El Chichón (1980), Mount St. Helens (1982), and Pinatubo (1991), as indicated in Fig. 11. Large

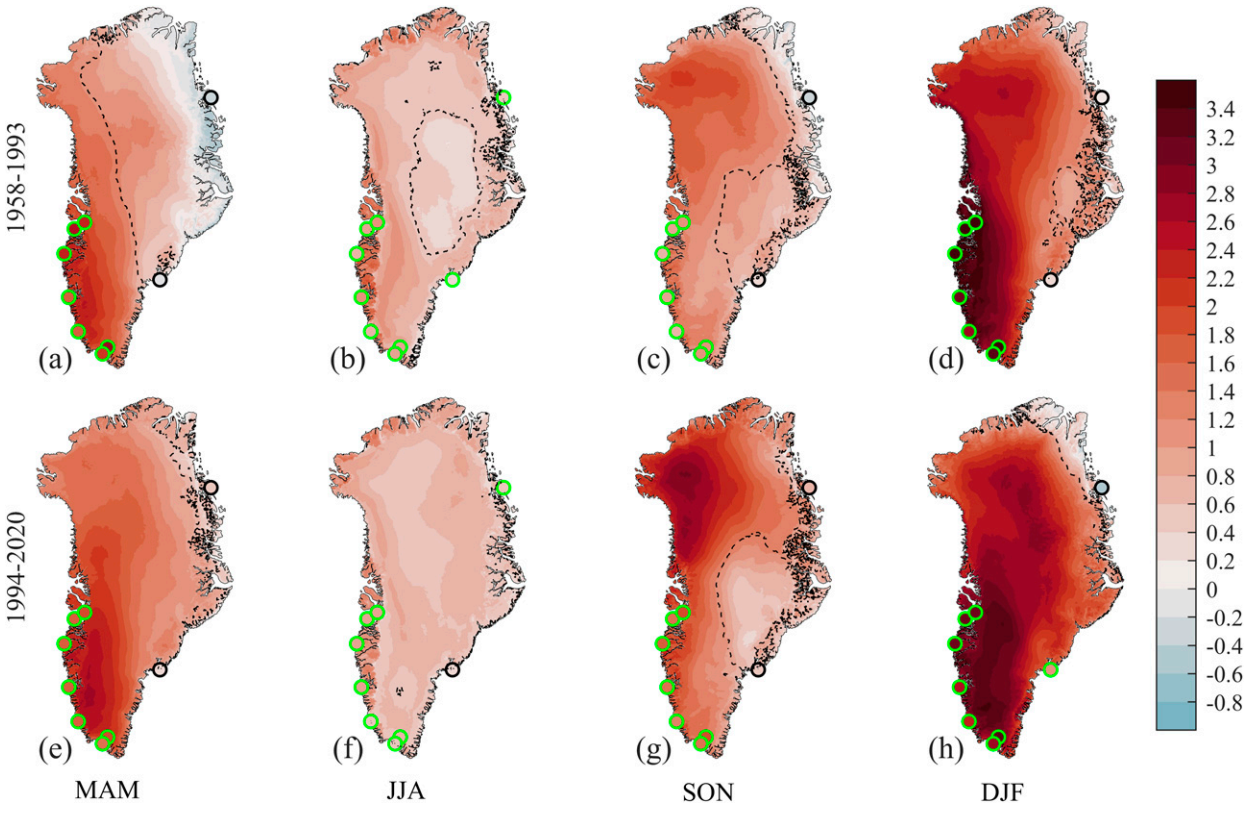

FIG. 9. The spatial distribution of the slope (°C perσ GBI) of the linear regression between seasonal T2m from RACMO2 and GBI. The regression slope maps show the T2m change for a 1 std dev change in GBI. Shown are the periods (a)–(d) 1958–93 and (e)–(h) 1994–2020. The dashed line represents the 95% significance level contour. The dots represent DMI stations, using the same color scale. For stations, the green circle indicates that the trend passes the 95% significance test.

amounts of sulfate aerosols injected into the stratosphere following large volcanic eruptions in the tropical Pacific Ocean lead to different temperature responses in different regions (Robock 2000). In Greenland, this results in a notable cooling (Kobashi et al. 2017), as confirmed in Fig. 11, where each eruption is followed by cooling in the following year. It has been shown that increased stratospheric volcanic aerosol loading intensifies the polar vortices, shifting the NAO into its positive phase (Stenchikov et al. 2002; Christiansen 2008; Wunderlich and Mitchell 2017), further enhancing cold conditions in Greenland in the following year. Box (2002) found that the cooling still persisted in Greenland after removing the NAO signal, possibly related to the direct cooling effect of enhanced aerosol concentrations.

The shift to positive GBI and negative NAO after 1994 initiated a multidecadal period of warm conditions and enhanced melt, especially in western Greenland. More frequent and stronger high pressure blocking over Greenland means increasing anticyclonic conditions over western Greenland (Mioduszewski et al. 2016). Since the 1990s, the number of anticyclonic blocking events has doubled (Fettweis et al. 2013), resulting in warm air masses from the south being frequently advected northward along the western side of the GrIS (Tedesco and Fettweis 2020). As a result, the western regions warm faster in summer than the east (Fig. 6b), in line with Hanna et al. (2012). The associated high temperatures and clear skies lead to strongly enhanced ice sheet melt rates, especially in western Greenland (Hanna et al. 2016). Under blocking conditions, air masses cross the northern GrIS to the northeast, regionally resulting in foehn conditions. Mattingly et al. (2018) found that this possibly caused of the largest melt event in the northeast in JJA of the past 20 years. Figure 5a shows that after 1994 the north of Greenland was warming faster than the south. A possible reason is the northward movement of the blocking pattern (Rajewicz and Marshall 2014; McLeod and Mote 2016), enhancing the sensitivity to the GBI in the north, especially in SON when it increased from 1.4°C perσ GBI to 2°C per σ GBI.

Although it has been shown that volcanic activity can affect the NAO/GBI in the short-term period, causes of multidecadal atmospheric circulation anomalies remain elusive. For instance, the connection between NAO and Atlantic multidecadal variability (AMV) remains a contentious issue (Keenlyside et al. 2016; Klavans et al. 2019). Davini et al. (2015) showed that a negative or positive NAO phase was often accompanied by the positive or negative AMV phase, respectively. In addition, it has been reported that the multidecadal Atlantic meridional overturning circulation also impacts NAO by affecting AMV (Zhang et al. 2019). The various AMV indices all show that

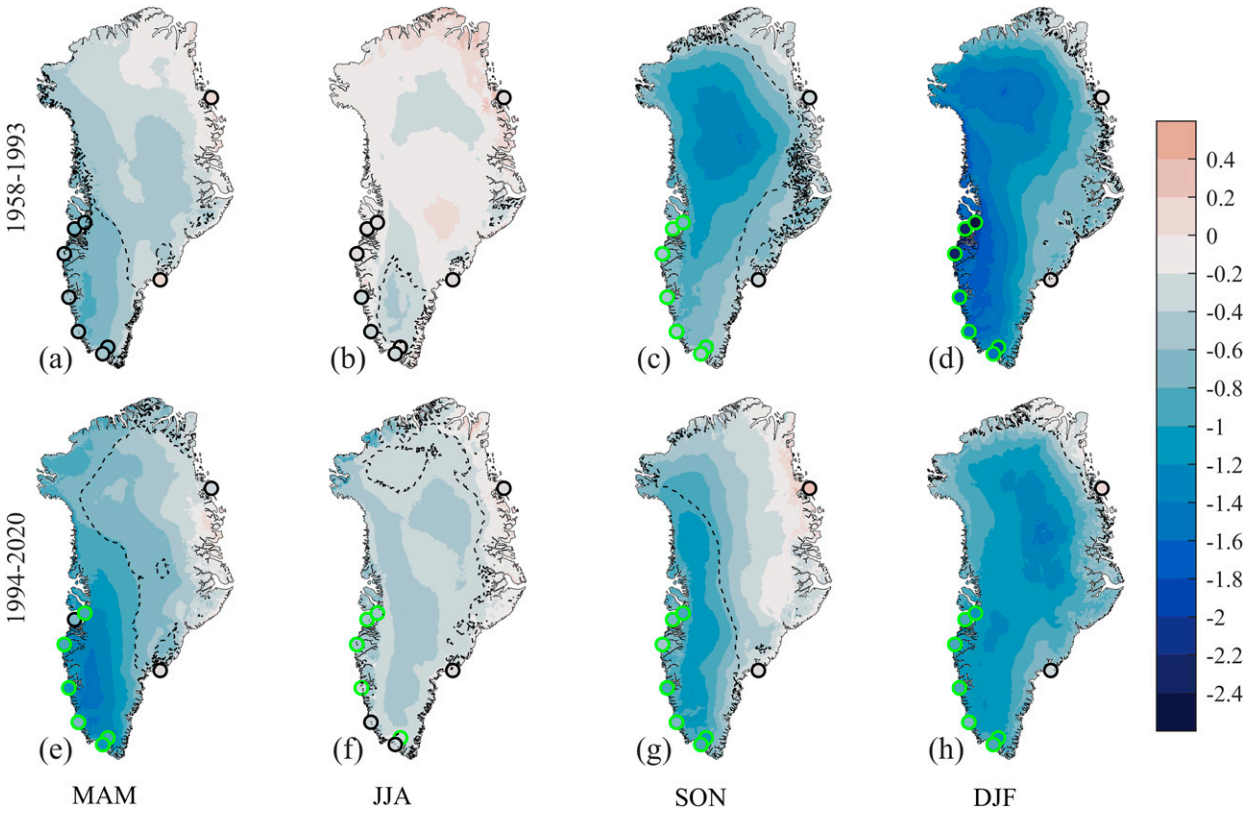

FIG. 10. As in Fig. 8, but for the slope (°C per σ NAO) of the linear regression between seasonal T2m from RACMO2 and NAO.

AMV has changed into a continuous positive phase since the mid-1990s (Peings et al. 2016). This is consistent with the continuous negative phase of NAO since that time and suggests that AMV indirectly influences interdecadal changes in Greenland T2m by regulating NAO/GBI. Moreover, the forcing effect of volcanic eruptions on NAO discussed previously is also amplified by the AMV negative phase (Ménégoz et al. 2018), leading to amplified cooling in Greenland.

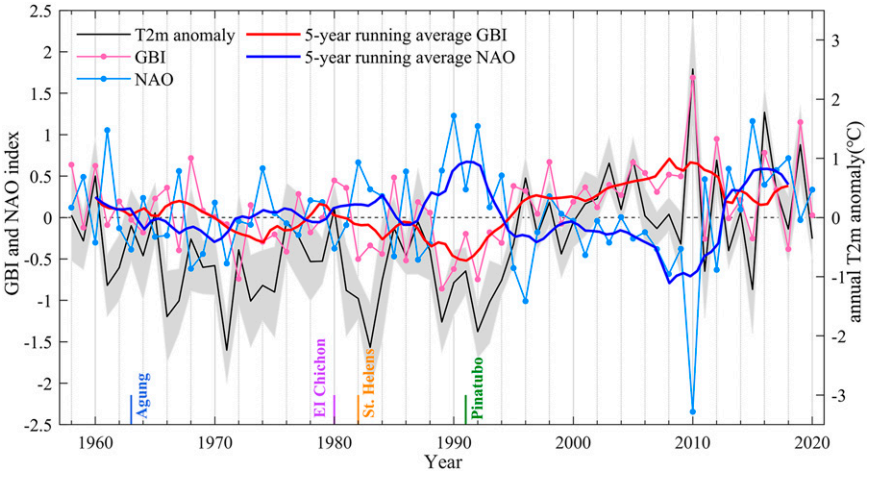

FIG. 11. Four volcanic eruptions and time series of GBI and NAO index 1958–2020, with 5-yr running means of both series. The black line represents annual Greenland T2m anomaly from RACMO2 relative to the 1991–2020 base period. The shaded area represents the standard deviation range.

Although since 2011 GBI and NAO have shifted toward, respectively, a more negative and a more positive phase, they have also remained highly variable, with recently more modest values and reduced warming. Ruan et al. (2019) suggested that this could temporarily slow down but likely not stop the future long-term warming in Greenland and mass loss of the GrIS. As shown in Fig. 11, recent variability in NAO and GBI predominantly promotes warming. Although CMIP5 and CMIP6 projections suggest a decrease of the GBI until 2100 (Delhasse et al. 2021), the models severely underestimate contemporary blocking frequency, making these modeled trends and variability uncertain. Therefore, the future trend of Greenland T2m and the role played by the large-scale circulation currently remain uncertain.

6. Conclusions

Near-surface air temperature (T2m), especially summer T2m, to a large extent determines the length and intensity of the melt season in Greenland, affecting the mass balance of the ice sheet. In this study, we use observed T2m from DMI stations in the ice-free coastal zone and PROMICE AWS on the ice sheet to evaluate the atmospheric reanalysis ERA5 and the regional climate model RACMO2.3p2 over Greenland. We use the latter product to show that Greenland warming is well represented by a temperature jump of ~1°C in 1994, with relatively constant temperatures before and after. The southwest was the region with the strongest negative T2m anomaly before 1994, whereas the northeast shows a persistent temperature increase after 1994. In terms of seasonal and regional differences in temperature changes, winter shows the strongest warming in 1994. The regional influence of the large-scale circulation, represented by the indices for NAO and GBI, on T2m and changes therein is very strong. The region with the strongest sensitivity is the southwest, with the influence gradually weakening toward the northeast and even weakly reversed in the far coastal northeast.

Future research on near-surface air temperature changes in Greenland should focus on further elucidating these complex relationships that either enhance or limit the response of Greenland climate to global warming.

Acknowledgments. This work was funded by the Natural Science Foundation of China (42171121 and 41701059) and the Postdoctoral Science Foundation of China (40411594). The authors gratefully acknowledge support from data availability from PROMICE and from the ERA5 reanalysis projects of the ECMWF. The authors thank Brice Noël (Utrecht University) for RACMO2.3p2 data support and Edward Hanna (University of Lincoln) for monthly GBI data support. Author van den Broeke acknowledges support of the Netherlands Earth System Science Centre (NESSC).

Data availability statement. The PROMICE observations are available online (http://promice.org/download-data/). The DMI observations are available online (https://www.dmi.dk/publikationer/). The ERA5 data used in this study are openly available from ECMWF (https://www.ecmwf.int/en/forecasts/datasets/browse-reanalysis-datasets). Both GBI (https://psl.noaa.gov/data/timeseries/daily/GBI/) and NAO (https://psl.noaa.gov/data/timeseries/daily/NAO/) data are available online. All results and the script of the whole processes are available through an email request to the authors.

REFERENCES

Abdalati, W., and K. Steffen, 1997: The apparent effects of the Mt. Pinatubo eruption on the Greenland ice sheet melt extent. *Geophys. Res. Lett.*, **24**, 1795–1797, https://doi.org/10.1029/97GL01706.

Abermann, J., B. Hansen, M. Lund, S. Wacker, M. Karami, and J. Cappelen, 2017: Hotspots and key periods of Greenland climate change during the past six decades. *Ambio*, **46**, 3–11, https://doi.org/10.1007/s13280-016-0861-y.

Bell, B., and Coauthors, 2020: ERA5 monthly averaged data on single levels from 1950 to 1978 (preliminary version). Copernicus Climate Change Service (C3S) Climate Data Store (CDS), accessed 11 November 2020, https://cds.climate.copernicus-climate.eu/cdsapp#!/dataset/reanalysis-era5-single-levels-monthly-means-preliminary-back-extension?tab=overview.

Box, J. E., 2002: Survey of Greenland instrumental temperature records: 1873–2001. *Int. J. Climatol.*, **22**, 1829–1847, https://doi.org/10.1002/joc.852.

——, L. Yang, D. H. Bromwich, and L. S. Bai, 2009: Greenland ice sheet surface air temperature variability: 1840–2007. *J. Climate*, **22**, 4029–4049, https://doi.org/10.1175/2009JCLI2816.1.

——, and Coauthors, 2011: Greenland [in "State of the Climate in 2010"]. *Bull. Amer. Meteor. Soc.*, **92** (6), 161–171, https://doi.org/10.1175/1520-0477-92.6.S1.

Buch, E., S. A. Pedersen, and M. H. Ribergaard, 2004: Ecosystem variability in West Greenland waters. *J. Northwest Atl. Fish. Sci.*, **34**, 13–28, https://doi.org/10.2960/J.v34.m479.

Cappelen, J., Ed., 2021: Weather observations from Greenland 1958–2020. Danish Meteorological Institute Tech. Rep. 21-08, DMI, Ministry of Transport, Copenhagen, Denmark, 20 pp., https://www.dmi.dk/publikationer/.

——, B. V. Jørgensen, E. V. Laursen, L. S. Stannius, and R. S. Thomsen, 2001: The observed climate of Greenland, 1958–99—With climatological standard normals, 1961–90. Danish Meteorological Institute Tech. Rep. 00-18, DMI, 152 pp.

Christiansen, B., 2008: Volcanic eruptions, large-scale modes in the Northern Hemisphere, and the El Niño–Southern Oscillation. *J. Climate*, **21**, 910–922, https://doi.org/10.1175/2007JCLI1657.1.

Christensen, T. R., M. F. Arndal, and E. Topp-Jørgensen, 2018: Greenland ecosystem monitoring annual report cards 2017. Danish Centre for Environment and Energy, Aarhus University, 44 pp.

Chylek, P., M. K. Dubey, and G. Lesins, 2006: Greenland warming of 1920–1930 and 1995–2005. *Geophys. Res. Lett.*, **33**, L11707, https://doi.org/10.1029/2006GL026510.

Colgan, W., and Coauthors, 2019: Greenland ice sheet mass balance assessed by PROMICE (1995–2015). *Geol. Surv. Denmark Greenl. Bull.*, **43**, e2019430201, https://doi.org/10.34194/GEUSB-201943-02-01.

Comiso, J. C., 2003: Warming trends in the Arctic from clear sky satellite observations. *J. Climate*, **16**, 3498–3510, https://doi.org/10.1175/1520-0442(2003)016<3498:WTITAF>2.0.CO;2.

Davini, P., C. Cagnazzo, R. Neale, and J. Tribbia, 2012: Coupling between Greenland blocking and the North Atlantic Oscillation pattern. *Geophys. Res. Lett.*, **39**, L14701, https://doi.org/10.1029/2012GL052315.

——, J. von Hardenberg, and S. Corti, 2015: Tropical origin for the impacts of the Atlantic multidecadal variability on the Euro-Atlantic climate. *Environ. Res. Lett.*, **10**, 094010, https://doi.org/10.1088/1748-9326/10/9/094010.

Delhasse, A., C. Kittel, C. Amory, S. Hofer, D. van As, R. S. Fausto, and X. Fettweis, 2020: Brief communication: Evaluation of the near-surface climate in ERA5 over the Greenland ice sheet. *Cryosphere*, **14**, 957–965, https://doi.org/10.5194/tc-14-957-2020.

——, E. Hanna, C. Kittel, and X. Fettweis, 2021: Brief communication: CMIP6 does not suggest any atmospheric blocking increase in summer over Greenland by 2100. *Int. J. Climatol.*, **41**, 2589–2596, https://doi.org/10.1002/joc.6977.

Dethloff, K., A. Rinke, R. Lehmann, J. H. Christensen, M. Botzet, and B. Machenhauer, 1996: Regional climate model of the Arctic atmosphere. *J. Geophys. Res.*, **101**, 23 401–23 422, https://doi.org/10.1029/96JD02016.

ECMWF, 2018: What are the changes from ERA-Interim to ERA5? Accessed 6 March 2020, https://confluence.ecmwf.int//pages/viewpage.action?pageId=74764925.

Espinoza, J. C., and Coauthors, 2019: Regional hydro-climatic changes in the southern Amazon Basin (upper Madeira Basin) during the 1982–2017 period. *J. Hydrol. Reg. Stud.*, **26**, 100637, https://doi.org/10.1016/j.ejrh.2019.100637.

Fang, Z. F., 2004: Statistical relationship between the Northern Hemisphere sea ice and atmospheric circulation during wintertime. *Observation, Theory and Modeling of Atmospheric Variability*, World Scientific Publishing, 131–141.

Fausto, R. S., and Coauthors, 2021: PROMICE automatic weather station data. *Earth Syst. Sci. Data Discuss.*, https://doi.org/10.5194/essd-2021-80.

Fettweis, X., E. Hanna, C. Lang, A. Belleflamme, M. Erpicum, and H. Gallée, 2013: Brief communication: Important role of the mid-tropospheric atmospheric circulation in the recent surface melt increase over the Greenland ice sheet. *Cryosphere*, **7**, 241–248, https://doi.org/10.5194/tc-7-241-2013.

——, and Coauthors, 2017: Reconstructions of the 1900–2015 Greenland ice sheet surface mass balance using the regional climate MAR model. *Cryosphere*, **11**, 1015–1033, https://doi.org/10.5194/tc-11-1015-2017.

Hanna, E., and J. Cappelen, 2003: Recent cooling in coastal southern Greenland and relation with the North Atlantic Oscillation. *Geophys. Res. Lett.*, **30**, 1132, https://doi.org/10.1029/2002GL015797.

——, and Coauthors, 2008: Increased runoff from melt from the Greenland ice sheet: A response to global warming. *J. Climate*, **21**, 331–341, https://doi.org/10.1175/2007JCLI1964.1.

——, S. H. Mernild, J. Cappelen, and K. Steffen, 2012: Recent warming in Greenland in a long-term instrumental (1881–2012) climatic context: I. Evaluation of surface air temperature records. *Environ. Res. Lett.*, **7**, 045404, https://doi.org/10.1088/1748-9326/7/4/045404.

——, T. E. Cropper, P. D. Jones, A. A. Scaife, and R. Allan, 2015: Recent seasonal asymmetric changes in the NAO (a marked summer decline and increased winter variability) and associated changes in the AO and Greenland blocking index. *Int. J. Climatol.*, **35**, 2540–2554, https://doi.org/10.1002/joc.4157.

——, ——, R. J. Hall, and J. Cappelen, 2016: Greenland blocking index 1851–2015: A regional climate change signal. *Int. J. Climatol.*, **36**, 4847–4861, https://doi.org/10.1002/joc.4673.

——, and Coauthors, 2018: Greenland blocking index daily series 1851–2015: Analysis of changes in extremes and links with North Atlantic and UK climate variability and change. *Int. J. Climatol.*, **38**, 3546–3564, https://doi.org/10.1002/joc.5516.

——, and Coauthors, 2021: Greenland surface air temperature changes from 1981 to 2019 and implications for ice-sheet melt and mass-balance change. *Int. J. Climatol.*, **41**, E1336–E1352, https://doi.org/10.1002/joc.6771.

Hersbach, H., and D. Dee, 2016: ERA5 reanalysis is in production. *ECMWF Newsletter*, No. 147, ECMWF, Reading, United Kingdom, 7, http://www.ecmwf.int/sites/default/files/elibrary/2016/16299-newsletter-no147-spring-2016.pdf.

Hofer, S., A. J. Tedstone, X. Fettweis, and J. L. Bamber, 2017: Decreasing cloud cover drives the recent mass loss on the Greenland ice sheet. *Sci. Adv.*, **3**, e1700584, https://doi.org/10.1126/sciadv.1700584.

Howat, I. M., A. Negrete, and B. E. Smith, 2014: The Greenland Ice Mapping Project (GIMP) land classification and surface elevation data sets. *Cryosphere*, **8**, 1509–1518, https://doi.org/10.5194/tc-8-1509-2014.

Hurrell, J. W., 1995: Decadal trends in the North Atlantic Oscillation: Regional temperatures and precipitation. *Science*, **269**, 676–679, https://doi.org/10.1126/science.269.5224.676.

Ilori, O. W., and V. O. Ajayi, 2020: Change detection and trend analysis of future temperature and rainfall over West Africa. *Earth Syst. Environ.*, **4**, 493–512, https://doi.org/10.1007/s41748-020-00174-6.

Jiang, S., A. Ye, and C. Xiao, 2020: The temperature increase in Greenland has accelerated in the past five years. *Global Planet. Change*, **194**, 103297, https://doi.org/10.1016/j.gloplacha.2020.103297.

Jones, P. D., T. Jónsson, and D. Wheeler, 1997: Extension to the North Atlantic Oscillation using early instrumental pressure observations from Gibraltar and south-west Iceland. *Int. J. Climatol.*, **17**, 1433–1450, https://doi.org/10.1002/(SICI)1097-0088(19971115)17:13<1433::AID-JOC203>3.0.CO;2-P.

Keenlyside, N. S., J. Ba, J. Mecking, N. E. Omrani, M. Latif, R. Zhang, and R. Msadek, 2016: North Atlantic multi-decadal variability—Mechanisms and predictability. *Climate Change: Multidecadal and Beyond*, World Scientific, 141–157.

Klavans, J. M., A. C. Clement, and M. A. Cane, 2019: Variable external forcing obscures the weak relationship between the NAO and North Atlantic multidecadal SST variability. *J. Climate*, **32**, 3847–3864, https://doi.org/10.1175/JCLI-D-18-0409.1.

Kobashi, T., and Coauthors, 2017: Volcanic influence on centennial to millennial Holocene Greenland temperature change. *Sci. Rep.*, **7**, 1441, https://doi.org/10.1038/s41598-017-01451-7.

Mattingly, K. S., T. L. Mote, and X. Fettweis, 2018: Atmospheric river impacts on Greenland ice sheet surface mass balance. *J. Geophys. Res. Atmos.*, **123**, 8538–8560, https://doi.org/10.1029/2018JD028714.

McCormick, M. P., L. W. Thomason, and C. R. Trepte, 1995: Atmospheric effects of the Mt Pinatubo eruption. *Nature*, **373**, 399–404, https://doi.org/10.1038/373399a0.

McLeod, J. T., and T. L. Mote, 2016: Linking interannual variability in extreme Greenland blocking episodes to the recent increase in summer melting across the Greenland ice sheet. *Int. J. Climatol.*, **36**, 1484–1499, https://doi.org/10.1002/joc.4440.

Ménégoz, M., C. Cassou, D. Swingedouw, Y. Ruprich-Robert, P. A. Bretonnière, and F. Doblas-Reyes, 2018: Role of the Atlantic multidecadal variability in modulating the climate response to a Pinatubo-like volcanic eruption. *Climate Dyn.*, **51**, 1863–1883, https://doi.org/10.1007/s00382-017-3986-1.

Mernild, S. H., E. Hanna, J. C. Yde, J. Cappelen, and J. K. Malmros, 2014: Coastal Greenland air temperature extremes and trends 1890–2010: Annual and monthly analysis. *Int. J. Climatol.*, **34**, 1472–1487, https://doi.org/10.1002/joc.3777.

Mioduszewski, J. R., A. K. Rennermalm, A. Hammann, M. Tedesco, E. U. Noble, J. C. Stroeve, and T. L. Mote, 2016: Atmospheric drivers of Greenland surface melt revealed by self-organizing maps. *J. Geophys. Res. Atmos.*, **121**, 5095–5114, https://doi.org/10.1002/2015JD024550.

Moon, T. A., and Coauthors, 2020: Arctic Report Card 2020: Greenland Ice Sheet. Administrative Rep., NOAA, 9 pp., https://doi.org/10.25923/ms78-g612.

Nghiem, S. V., and Coauthors, 2012: The extreme melt across the Greenland ice sheet in 2012. *Geophys. Res. Lett.*, **39**, L20502, https://doi.org/10.1029/2012GL053611.

Noël, B., W. J. van de Berg, E. van Meijgaard, P. Kuipers Munneke, R. S. W. van de Wal, and M. R. van den Broeke, 2015: Evaluation of the updated regional climate model RACMO2.3: Summer snowfall impact on the Greenland ice sheet. *Cryosphere*, **9**, 1831–1844, https://doi.org/10.5194/tc-9-1831-2015.

——, and Coauthors, 2018: Modelling the climate and surface mass balance of polar ice sheets using RACMO2—Part 1: Greenland (1958–2016). *Cryosphere*, **12**, 811–831, https://doi.org/10.5194/tc-12-811-2018.

——, W. J. van de Berg, S. Lhermitte, and M. R. van den Broeke, 2019: Rapid ablation zone expansion amplifies north Greenland mass loss. *Sci. Adv.*, **5**, eaaw0123, https://doi.org/10.1126/sciadv.aaw0123.

——, and Coauthors, 2020: Brief communication: CESM2 climate forcing (1950–2014) yields realistic Greenland ice sheet surface mass balance. *Cryosphere*, **14**, 1425–1435, https://doi.org/10.5194/tc-14-1425-2020.

Orsi, A., and Coauthors, 2017: The recent warming trend in North Greenland. *Geophys. Res. Lett.*, **44**, 6235–6243, https://doi.org/10.1002/2016GL072212.

Peings, Y., G. Simpkins, and G. Magnusdottir, 2016: Multidecadal fluctuations of the North Atlantic Ocean and feedback on the winter climate in CMIP5 control simulations. *J. Geophys. Res. Atmos.*, **121**, 2571–2592, https://doi.org/10.1002/2015JD024107.

Pettitt, A. N., 1979: A non-parametric approach to the change-point problem. *J. Roy. Stat. Soc.*, **28C**, 126–135, https://doi.org/10.2307/2346729.

Rajewicz, J., and S. J. Marshall, 2014: Variability and trends in anticyclonic circulation over the Greenland ice sheet, 1948–2013. *Geophys. Res. Lett.*, **41**, 2842–2850, https://doi.org/10.1002/2014GL059255.

Reeves Eyre, J. E., and X. Zeng, 2017: Evaluation of Greenland near surface air temperature datasets. *Cryosphere*, **11**, 1591–1605, https://doi.org/10.5194/tc-11-1591-2017.

Robock, A., 2000: Volcanic eruptions and climate. *Rev. Geophys.*, **38**, 191–219, https://doi.org/10.1029/1998RG000054.

Rogers, J. C., 1984: The association between the North Atlantic Oscillation and the Southern Oscillation in the Northern Hemisphere. *Mon. Wea. Rev.*, **112**, 1999–2015, https://doi.org/10.1175/1520-0493(1984)112<1999:TABTNA>2.0.CO;2.

Ruan, R., and Coauthors, 2019: Decelerated Greenland ice sheet melt driven by positive summer North Atlantic Oscillation. *J. Geophys. Res. Atmos.*, **124**, 7633–7646, https://doi.org/10.1029/2019JD030689.

Serreze, M. C., and J. A. Francis, 2006: The Arctic amplification debate. *Climatic Change*, **76**, 241–264, https://doi.org/10.1007/s10584-005-9017-y.

Steffen, K., J. E. Box, and W. Abdalati, 1996: Greenland climate network: GC-Net. US Army Cold Regions Reattach and Engineering (CRREL), CRREL Special Rep., 98–103.

Stenchikov, G., A. Robock, V. Ramaswamy, M. D. Schwarzkopf, K. Hamilton, and S. Ramachandran, 2002: Arctic Oscillation response to the 1991 Mount Pinatubo eruption: Effects of volcanic aerosols and ozone depletion. *J. Geophys. Res.*, **107**, 4803, https://doi.org/10.1029/2002JD002090.

Tedesco, M., and X. Fettweis, 2020: Unprecedented atmospheric conditions (1948–2019) drive the 2019 exceptional melting season over the Greenland ice sheet. *Cryosphere*, **14**, 1209–1223, https://doi.org/10.5194/tc-14-1209-2020.

——, and Coauthors, 2016: Arctic cut-off high drives the poleward shift of a new Greenland melting record. *Nat. Commun.*, **7**, 11723, https://doi.org/10.1038/ncomms11723.

——, and Coauthors, 2018: Greenland ice sheet [in "State of the Climate in 2017"]. *Bull. Amer. Meteor. Soc.*, S152–S156, https://doi.org/10.1175/2018BAMSStateoftheClimate.1.

van de Berg, W. J., and B. Medley, 2016: Brief communication: Upper-air relaxation in RACMO2 significantly improves modelled interannual surface mass balance variability in Antarctica. *Cryosphere*, **10**, 459–463, https://doi.org/10.5194/tc-10-459-2016.

van den Broeke, M., and Coauthors, 2017: Greenland ice sheet surface mass loss: Recent developments in observation and modeling. *Curr. Climate Change Rep.*, **3**, 345–356, https://doi.org/10.1007/s40641-017-0084-8.

——, J. Bamber, J. Ettema, E. Rignot, E. Schrama, W. J. van de Berg, E. van Meijgaard, I. Velicogna, and B. Wouters, 2009: Partitioning recent Greenland mass loss. *Science*, **326**, 984–986, https://doi.org/10.1126/science.1178176.

van Loon, H., and J. C. Rogers, 1978: The seesaw in winter temperatures between Greenland and northern Europe. Part I: General description. *Mon. Wea. Rev.*, **106**, 296–310, https://doi.org/10.1175/1520-0493(1978)106<0296:TSIWTB>2.0.CO;2.

Wunderlich, F., and D. M. Mitchell, 2017: Revisiting the observed surface climate response to large volcanic eruptions. *Atmos. Chem. Phys.*, **17**, 485–499, https://doi.org/10.5194/acp-17-485-2017.

Zhang, R., and Coauthors, 2019: A review of the role of the Atlantic meridional overturning circulation in Atlantic multidecadal variability and associated climate impacts. *Rev. Geophys.*, **57**, 316–375, https://doi.org/10.1029/2019RG000644.